Swansea University
Prifysgol Abertawe

Cronfa
Setting Research Free

Cronfa - Swansea University Open Access Repository

This is an author produced version of a paper published in :
Surface and Coatings Technology

Cronfa URL for this paper:
http://cronfa.swan.ac.uk/Record/cronfa26470

Paper:
Berry, L., Phillips, C. & Penney, D. (2016). Understanding the role of snout contamination in the formation of an oxide based defect in hot dip galvanised coating. *Surface and Coatings Technology*

http://dx.doi.org/10.1016/j.surfcoat.2016.02.009

This article is brought to you by Swansea University. Any person downloading material is agreeing to abide by the terms of the repository licence. Authors are personally responsible for adhering to publisher restrictions or conditions. When uploading content they are required to comply with their publisher agreement and the SHERPA RoMEO database to judge whether or not it is copyright safe to add this version of the paper to this repository.
http://www.swansea.ac.uk/iss/researchsupport/cronfa-support/

Accepted Manuscript

Understanding the role of snout contamination in the formation of an oxide based defect in hot dip galvanised coating

Lewis J. Berry, Craig H. Phillips, David J. Penney

PII: S0257-8972(16)30071-8
DOI: doi: 10.1016/j.surfcoat.2016.02.009
Reference: SCT 20916

To appear in: *Surface & Coatings Technology*

Received date: 31 October 2015
Revised date: 29 January 2016
Accepted date: 2 February 2016

Please cite this article as: Lewis J. Berry, Craig H. Phillips, David J. Penney, Understanding the role of snout contamination in the formation of an oxide based defect in hot dip galvanised coating, *Surface & Coatings Technology* (2016), doi: 10.1016/j.surfcoat.2016.02.009

This is a PDF file of an unedited manuscript that has been accepted for publication. As a service to our customers we are providing this early version of the manuscript. The manuscript will undergo copyediting, typesetting, and review of the resulting proof before it is published in its final form. Please note that during the production process errors may be discovered which could affect the content, and all legal disclaimers that apply to the journal pertain.

Understanding the role of snout contamination in the formation of an oxide based defect in hot dip galvanised coating

Lewis J. Berry[1], Craig H. Phillips[2], David J. Penney[3]

[1,3] The Materials and Manufacturing Academy, College of Engineering, Swansea University, Bay Campus, Swansea SA1 8QQ, UK

Phone: +44 (0) 7885826063 Email: lewis.berry@tatasteel.com; 748386@swansea.ac.uk

Phone: +44 (0) 1792 606706 Email: D.Penney@swansea.ac.uk

[2] ZODIAC, Tata Steel Llanwern

Tata Steel Strip Products, Newport NP19 4QZ, UK

Phone: +44 (0) 01633 290011 Email: Craig.H.Phillips@tatasteel.com;

ACCEPTED MANUSCRIPT

ABSTRACT

Due to increased demand for defect free, quality critical outer panel material for the automotive sector, continued focus on zinc coating quality is required. The snout area of a continuous galvanizing line is often a major source of coating issues with various surface defects arising from poorly understood and uncontrolled snout practices. This paper investigates the formation of a snout defect termed 'the arrowhead defect', named after its characteristic arrowhead shape. Defective samples have been characterised with use of SEM/EDX and XRD and compared with contamination sources collected from within the continuous galvanising line snout. It is common practice to inject wet HNx into the snout in order to inhibit the production of zinc vapour. The wet HNx promotes the formation of a ZnO layer on the surface of the liquid zinc bath, preventing vaporisation and thereby reduces zinc dust contamination. The presence of ZnO, deliberately formed through the injection of wet HNx into the snout was observed within the arrowhead defect and can be identified as the root cause of this defect. Discrete contamination particles were entrained within the tail of the defect. XRD patterns of both the defect & snout contamination have been presented to discern the nature of the contamination entrained within the zinc coating. Characteristic ZnO peaks

were observed at $\theta=32^{o}$ for both surface contamination and at increasing penetration depths within the coating in the region of the arrowhead defect. The inclusion of the arrowhead defect in Full finish material led to an increase in the rate of corrosion 2.5x that of the corrosion rate on non-defective material, highlighting the need to produce defect free galvanized steel for both aesthetic and corrosion purposes. Whilst the injection of wet HNx as a method of suppressing the formation of zinc vapour is a long standing process for automotive Full Finish production, due to the nature of these oxide based defects, this process is in fact a "double edged sword" in that it solves one problem but can create another. Alternative techniques to supress zinc vapour formation should be investigated to further drive up the quality of zinc coatings for automotive applications.

Keywords: Zinc, XRD, WLI, GI Full Finish, Coating Quality, Continuous Hot dip Galvanizing

ACCEPTED MANUSCRIPT

1. INTRODUCTION

The increased usage of GI full finish galvanized coated steel sheet for exposed outer body automotive panels has led to the need for improved surface quality. The coating section (from extension chamber to the gas knives) of a Continuous Galvanizing Line (CGL) [1] is the source of numerous defects and various processes have been introduced in order to improve surface quality. The study of defective galvanized coatings has been paramount in understanding of defect formation and in developing strategies to improve surface quality [2, 3]. Due to an ever increasing need to improve surface quality of the GI Full Finish products, further comprehensive characterisation of defective zinc coatings have been undertaken [4-6] acting as a basis for quality centred process improvement. The production of zinc vapour under a reducing HNx atmosphere within the snout [7] along with the formation of intermetallic dross [8] are two of the primary origins of coating defects. Whilst the formation of intermetallic dross particles are still a major source of defective coatings, the introduction

of wet HNx snout atmospheres have all but eradicated defects that originate from zinc evaporation [7]. Zinc evaporation is undesirable since gaseous zinc will condense in the snout area and contaminate the incoming steel strip. The subsequent zinc particles alloy with the steel surface, forming FeZn intermetallics that are not readily wetted by the liquid zinc [7]. The dew point, typically around -24^{o}C, within the snout is a result of the injection of wet HNx which promotes the formation of a barrier layer of zinc oxide on the surface of the zinc bath within the snout, as indicated in Fig. 1, supressing zinc evaporation. The introduction of wet HNx into the snout and the subsequent decrease in zinc evaporation to very low levels has been previously described [7, 9]. The relationship between the injected dew point of wet HNx and the formation of bare spots was investigated by Arnold and Kim et al. The formation of bare spots was found to be due to the development of localised surface intermetallics formed through interactions between the moving steel and zinc vapour. Saint-Raymond et al [10] defined the relationship between exposed surface area of molten zinc and the rate of formation of zinc vapour (eqn. 1).

$$J_{Zn} = \alpha S_{evap} \left[{P_{Zn}}^{Sat}(T_{bath}) - P_{Zn} \right] \quad \text{(eqn. 1)}$$

Where J_{Zn} = Zinc evaporation rate

S_{evap} = Evaporation surface area

T_{bath} = Bath temperature

P_{zn} = Zinc pressure

${P_{Zn}}^{Sat}$ = Zn saturation vapour pressure

α = Boundary layer diffusion constant

Upon the introduction of wet HNx, the S_{evap} term reduces to zero as does the theoretical Zn evaporation rate. However, the vaporisation of molten zinc may still be possible through breaks in the oxide barrier and needs to be further investigated in order to determine optimum snout conditions for the production of GI full finish. Whilst the introduction of wet HNx does act as a method of reducing zinc vapour formation, the uncontrolled formation of barrier

ACCEPTED MANUSCRIPT

oxides can themselves induce coating quality issues. If the zinc oxide barrier layer within the snout becomes unstable, zinc oxide particles break away and become entrained within the coating through the action of the rapidly moving steel strip, as shown in Fig. 1b. It is therefore necessary to control the size and thickness of the zinc oxide layer through the use of extraction techniques that remove the zinc and a portion of the oxide barrier layer from within the snout.

The use of pumps in the continuous removal of surface oxides formed produced through the introduction of wet HNx atmospheres was introduced by Becherer [11] and resulted in the elimination of zinc dust related defects. The Push/Pull surface cleanliness system was optimised by Phillips et al [12] utilizing water modelling to discern optimum settings for the removal of surface contamination. However, the use of a centrifugal snout pump Push/Pull type configuration can cause turbulence within the snout leading to interactions between the strip surface and the oxide layer, and as such new on line industrial techniques have been designed to continuously remove the surface dross layer [13].

1.1 Mechanism of Defect Formation

The mechanism of formation of the arrowhead defect can be observed with use of the snout camera. The attraction of surface oxides to the moving strip due to liquid zinc turbulence causes oxide entrainment within the galvanized coating as observed in Fig. 2 which shows the zinc bath surface inside the snout. Surface contamination is present at the extremities of the molten zinc surface. The movement of this contamination towards the moving strip can be observed readily, leading to the entrainment of this contamination in the coating. The uncontrolled formation and entrainment of surface oxides results in the creation of the arrowhead defect as observed by the Continuous Galvanizing Line surface quality camera system as highlighted in Fig. 3. The arrowhead defects are linked to the insufficient removal of barrier oxides from the snout surface. Achieving the correct balance between removing excess surface oxide and maintaining an inhibiting surface layer is complex. If the rate of removal drastically exceeds the rate of formation of the barrier oxide then an exposed surface

ACCEPTED MANUSCRIPT

of molten zinc will, increase the rate of formation of zinc vapour. This was described in detail by Arnold et al [7].

Contamination originating from around the snout area has been previously characterised [14] with a consideration for the effects on coating quality [15], whereby the inclusion of mixed $ZnAl_{2-x}Fe_yO_4$ spinel oxide by-products into the coating resulted in the formation of outbursts of intermetallics. However, the contamination characterised were limited to oxidic, bottom and blowing dross with no consideration of by-products formed within the snout. Furthermore, no characterisation has been achieved on a microscopic scale. This paper presents an overview of individual microscopic phenomena comprising snout surface oxides and how their presence can lead to defective galvanized coatings.

ACCEPTED MANUSCRIPT

1.2 GI Full Finish Sample collection

Arrowhead defective samples were collected from rejected GI Full Finish production material produced with a bath composition as shown in table 1, where Al wt.% bath content was measured with disposable Alzin probes and cross checked with spark Spectroscopy using an Ametek SPECTROMAXx Optical Emission Spectrometer. Control samples were obtained from non-defective material produced during the same shift of GI Full Finish material for direct comparison. The defective and non-defective material collected were both typical low carbon steels (3013 steel grade) with 7-10µm coating thickness.

1.3 Snout surface oxide sample collection

Snout surface oxides were collected upon removal of the dross pumps. Powdered samples with different morphologies, including the white surface oxide powder described later within this paper, were observed at the inlets to the pumps. The pump inlets are situated within the snout and set at the level of the molten zinc during production.

2. EXPERIMENTAL

2.1 Cross Sectional Analysis

Cross sections of both arrowhead defective and non-defective samples were taken to investigate the presence of coating contamination that may give rise to irregular surface topography. Samples were cross sectioned using a Beuhler IsoMet 5000 linear precision saw and polished to a 0.3μm finish using a 0.3μm Beuhler diamond based polishing suspension and Kemet Chem H polishing cloth on a Beuhler AutoMet 300 grinding/polishing machine.

2.2 Incremental etching

Arrowhead defective samples were incrementally etched in order to investigate the position of contamination within the thickness of the galvanized coating. The region of coating surrounding the arrowhead defect was indented with a Vickers hardness indenter as a method of coating weight determination and incrementally etched with 5% Nital (Nitric acid in Ethanol) at 2 second intervals as described by Penney et al [16]. The region of coating surrounding the arrowhead defect was indented with a Vickers hardness indenter in order to identify known regions of the sample that can be compared pre and post etch.

2.3 Scanning Electron Microscopy and Energy Dispersive X-ray Spectroscopy

Arrowhead defective samples were analysed using a Hitachi S-4800 Field Emission Gun Scanning Electron Microscope (FEG SEM) with an Oxford instruments Silicon Drift X-Max EDX Detector (SDD) and Inca EDX software to determine microstructure, morphology of arrowhead defective samples and to chemically characterise the nature of the galvanized coating.

For surface and cross sectional SEM imaging of arrowhead and non-defective samples, the detector settings were set to 15kV accelerating voltage and 20μA emission current to produce

ACCEPTED MANUSCRIPT

even contrast surface images of coating surface topography at a working distance of 8mm using the lower detector.

With use of BSE detector for backscatter SEM imaging of arrowhead defective samples to determine position of contamination relative to surface phenomena, the detector settings were set to 15kV accelerating voltage and 20µA emission current to produce high contrast bulk images of coating and contamination at a working distance of 5mm using the upper detector.

For EDX chemical characterisation of both surface and cross sectional arrowhead defective samples, the detector settings were set at 15kV accelerating voltage and 20µA emission current at a working distance of 15mm to maximise data acquisition for high quality EDX analysis.

2.4 White Light interferometry

Samples were analysed using a Bruker Wyko NT 9300 Optical Profiling System and subjected to a stitched scan with a scan length of 80µm and a back scan length of 40µm at 5x optical magnification. Samples were subjected to White Light Interferometry in order to quantify the nature of surface roughness and produce qualitative topographical maps for both arrowhead defective and non-defective samples.

2.5 X-Ray Diffraction

Samples were analysed with a Bruker D8 Discover Diffractomer using a Cu Kα radiation (λ = 0.15406nm) source in order to determine the chemical nature of the coating through non-destructive means. Both fixed and variable primary optic testing methods were employed in order to compare chemical surface and depth profiles of the GI Full Finish coating. For a variable primary optic testing, samples were subjected to an hour 11000 step D cycle with step parameters of 0.5 seconds per step and 0.0006^{o} increment per step between 5 and 80^{o}. For a fixed primary optic testing, the primary optic arm was fixed at 5^{o} intervals between 5-25^{o} and secondary optic arm varied from the initial primary arm setting to 80^{o} in order to give coating depth profiles at increasing penetration depths. The same time and incremental step profiles

ACCEPTED MANUSCRIPT

were used for both fixed and variable optic testing. XRD peak identification was carried out through use of the Open Crystallography Database.

2.6 Scanning Vibrating Electrode Technique (SVET)

The electrochemical characteristics of arrowhead defective and non-defective GI full finish were investigated with use of the SVET technique to determine the impact of the arrowhead defective on the corrosion performance of GI Full Finish material. Samples were immersed in 0.1% NaCl solution for 48 hours whilst subjected to surface corrosion mapping using the Swansea University SVET at hourly intervals. The principles of the technique, calibration of the SVET prior to scanning, post scan data manipulation to produce qualitative current density maps, the derivation of semi quantitative coating mass loss data [17] and possible applications to determine the nature of the corrosion of galvanized coating systems have been described elsewhere [18].

ACCEPTED MANUSCRIPT

3. RESULTS & DISCUSSION

3.1 Physical characteristics of the defect

The characteristic microscopic topography of the defect under SEM analysis can be shown to be a consequence of microfolding of the zinc coating, Fig. 4. This is consistent with that observed for the entrainment of other forms of contamination present during gas wiping [9]. The folding of the surface suggests the contamination present within the coating provides an obstacle to ideal coating weight control during wiping.

It is postulated that the mechanism for the formation of the arrowhead defect is formed by the wiping action of the gas knives. The high velocity gas impinges on the moving strip, wiping excess liquid zinc back down into the bath. When an entrained oxide passes through the gas wiping jet it prevents uniform flow of the liquid zinc back into the bath. Instead, liquid zinc is forced to flow around the particle, forming the characteristic arrow head shape. Furthermore, larger oxide particles can break up under the action of the wiping force and become entrained along the arrowhead contours resulting in the micro folding seen in Fig. 5. White light Interferometry was used to map the topography of the defective surface. The average surface roughness Ra for defective (2.01µm) and non-defective material (1.22µm) can be directly compared, however, consideration of Ra alone is not enough to determine the relationship between the entrainment of surface contamination and topographical effects. The comparison of the characteristic surface topography of the arrowhead defect with non-defective galvanized material is shown in Fig. 6. For the defective material an arrowhead like region of low surface roughness (Ra = 0.5µm) surrounds a region of greater surfae roughness throughout the body of the defect (Ra = 1.93µm). Regions of non-defective coating surrounding the defective region of the sample are comparable to defect free samples (Ra =

ACCEPTED MANUSCRIPT

1.24µm). It can be concluded that the increase in surface roughness within the body of the defect is due to greater temper roll roughness transfer bought about by differences in zinc coating thickness [19]. Furthermore, the interface between the zinc coating of normal surface roughness and regions of reduced roughness around the extremities of the defect have been linked to the presence of contamination within the coating.

3.2 Metallographic cross sections

In order to discern root cause of the arrowhead, defective and non-defective material were cross sectioned and polished to a 0.3µm finish before being subjected to SEM/EDX analysis. The substrate / Zn coating interface regions of non-defective material, Fig. 7, and arrowhead defective material, Fig. 7, were compared. Contamination at the interface between the substrate and Zn coating was clearly observed within the defective samples but not within the non-defective samples. EDX analysis of the contamination indicated regions of high concentrations of zinc and oxygen. The presence of zinc and oxygen containing species adjacent to the expected position of the Fe_2Al_5 interfacial layer suggests the entrainment of surface oxides from inside the snout. Previous instances of oxide containing defective coatings were investigated by Vlot [19] but associated with the entrainment of oxidized zinc vapour as opposed to the entrainment of zinc oxide material from the bath surface. No appreciable amount of aluminium was observed suggesting the formation of a ZnO barrier layer rather than $ZnAl_2O_4$, both of which would be possible given the typical dew point of injected wet HNx systems during galvanizing.

3.3 Incremental etching for contamination observation

The preferential dissolution of the Zn coating with retention of ceramic type species during etching has previously been observed and is a controllable method for the observation of oxide based contamination within a galvanized coating. Initial SEM/EDX was carried out over the arrowhead defect in order to compare the same region of the defect pre and post etch. Initial benchmarking of the defect showed regions of increased concentration of iron due to

ACCEPTED MANUSCRIPT

decreased zinc coating thickness and reduced surface roughness [19]. Regions of oxide associated with microfolding of the zinc coating can also be seen in Fig. 9, where green = Al, red = O, blue = Zn. After 8 seconds of incremental etching, particles of intermetallic top dross were observed dross within the body of the defect. EDX was used to confirm its chemical composition, as indicated in Fig 10. Whilst the majority of the sample was still covered by a thick zinc coating, at the head end of the defect the interfacial Fe_2Al_5 was exposed after a relatively short etching period. This is in agreement with phenomena described by Vlot et al [19] which showed regions of decreased surface roughness due to localised lower coating thicknesses. This suggests that the presence of the zinc oxide based contamination found at the coating substrate interface promotes micro folding and localised inhomogeneous coating thickness.

3.4 XRD characterisation of the arrowhead defect

The nature of the contamination observed within the zinc coating can be characterised with the use of X-Ray Diffraction (XRD). XRD analysis of the arrowhead defect containing Full Finish sample produced the X-ray diffractogram highlighted in Fig. 11.

The majority of the peaks observed within the arrowhead XRD spectra are associated with the zinc coating which dominate over the peaks associated with the contamination. Small contamination peaks have been characterised through comparison with known XRD scattering patterns of the types of contamination that would be observed around the snout of a galvanizing line [20-23], including the Fe_2Al_5 interfacial layer, intermetallic $Fe_2Al_5Zn_x$ top dross, zinc oxide (ZnO), alumina (Al_2O_3) and zinc aluminate ($ZnAl_2O_4$).

The smaller peaks were used to characterise the presence of the Fe_2Al_5 interfacial layer, zinc oxide and intermetallic dross within the tail of the arrowhead defect. Zinc oxide can be formed through two different mechanisms as indicated previously within the snout, through oxidation

ACCEPTED MANUSCRIPT

of the molten zinc surface with wet HNx or oxidation of zinc vapour, with only physical characteristics used to differentiate the nature of the contamination.

Through observation of the entrainment of snout surface oxides during production of material associated with the arrowhead defect, the investigation was focused on the characterisation of these oxides.

3.5 Electrochemical characterisation of the arrowhead defect

To determine the effect of the arrowhead defective coating on the corrosion resistance of the galvanized coating, a calibration factor ($1.29x10^{5}$ $Am^{-2}V^{-1}$) was obtained during calibration of the SVET and the microtip was scanned at a constant height of 100µm across the exposed corroding sample to directly compare post scan data for defective and non-defective material, whilst submerged in 0.1%NaCl electrolyte. Current density maps, indicating relative position and intensity of electrochemical phenomena occurring at the galvanized surface, were generated with use of cartography software (Surfer™ from golden Software) which show regions of localised anodic (shown in red) and general cathodic activity (shown in blue) across the period of immersion in electrolyte, Fig 12. For the duration of the immersion the non-defective regions of the coating afforded cathodic protection to the substrate. Increased anodic activity was observed around the position of the arrowhead defect. As the scan progressed, long lived anodic sites were observed around the extremities of the arrowhead defect due to decreased coating thickness at positions associated the microfolding of the zinc surface, in comparison with thicker coatings for the non-defective portions of the sample and roughened body of the defect.

Semi quantitative mass loss calculations have been compared for both defective and non-defective GI full finish. It is important to recognise that spatially resolved peak voltages are dependent upon scan height, and as such both arrowhead defective and non-defective samples were scanned at a constant height of 100µm to allow for direct comparison. Cumulative mass

ACCEPTED MANUSCRIPT

loss across the period of immersion indicated in Fig. 13, with arrowhead defective samples clearly showing an increase in corrosion rate, 2.5x that of normal GI full finish material. As such, the inclusion of arrowhead defective material in exposed automotive panels would lead to irregularity in the corrosion protection afforded by the metallic system and highlights the need to produce defect free GI Full Finish material.

ACCEPTED MANUSCRIPT

3.6 Snout surface oxide characterisation

Whilst characterisation of various Zn dust by products from the coating area of the galvanizing process has been undertaken both on pilot and production scale [7,9], little work has been undertaken to characterise the nature of production snout contamination on a microscopic level. Various complex morphologies comprising the snout surface oxide barrier formed as a result of wet HNx injection at the continuous galvanizing line were observed as indicated in Fig. 14 - 16. Previous characterisation of snout contamination was undertaken by Kim et al [9] on different zinc and oxygen containing compounds using ICP/XRD to determine stoichiometric composition. EDX was used to discern chemical composition of the white surface oxide. Fig. 15, where green = Al, red = O, blue = Zn, indicates the presence of large amounts of Zn and O in accordance with previous results. Furthermore, the observation of nanoscale ZnO rods/wires/flowers was observed. ZnO nanowire synthesis is of great interest due to the photo catalytic properties associated with the nanostructures. The properties of ZnO nanostructures have been well studied [24, 25]. It can be suggested that the nanostructures associated with the surface oxide forming via adsorption of Zn vapour onto the solid ZnO, although a more definitive mechanism of formation for the formation of flower like ZnO structures is provided by Pung et al [26]. Pung states that the formation of desirable ZnO geometries require carefully controlled reaction conditions. Under laboratory conditions, the reaction time, amount of the reactant present, and the choice of a suitable complexing agent are all crucial in the formation of desirable geometries. It is possible that local variation of

parameters such as dew point, the amount of wet HNx present, atmospheric temperature, residency time of the injected gas relative to the exposed molten zinc surface and cooling regime contribute to the formation of different ZnO morphologies with the snout of the galvanizing line, but is beyond the scope of this work and will form the basis of a separate study. The XRD diffractogram for the snout surface oxide contamination is presented in Fig. 17 as a direct comparison for the XRD spectra generated via analysis of the arrowhead defect, Fig 11.

The entrainment of the surface oxide type contamination was observed with use of the snout camera as indicated in Fig. 2 and with consideration of the XRD patterns produced by the arrowhead defect and the contamination collected from the snout, a consistent and distinct ZnO peak is observed at $\theta = 32$ at increased penetration depths, Fig. 18. Whilst the intensity of the ZnO peaks associated with other crystal planes are masked by the intensity of the zinc peaks, this distinct ZnO $[\bar{1},0,0]$ crystal plane is readily observed and confirms the presence of particles from the ZnO barrier layer within the arrowhead defect. This assignment is confirmed with analysis of the SEM/EDX cross sections and incrementally etched samples whereby discrete ZnO particles are observed within the zinc coating.

ACCEPTED MANUSCRIPT

4. METHODS OF DEFECT ELIMINATION

The formation of the arrowhead and other surface oxide based defects which manifest with different surface topography, can be minimised through the optimisation of snout pump process technology designed to attain control of over the cleanliness of the exposed molten zinc surface inside of the snout [12]. However, due to the nature of the wet HNx injection process on the continuous galvanizing line, if pumping methods were to fail during production this would results in increased occurrences of surface oxides based coating defects. Several methods have been developed to obviate the need for wet HNx injection as a method of zinc vapour suppression or to reduce the impact of zinc vapour that is formed during the process on the quality of the material produced.

A novel method of removing snout contamination, including both $Fe_2Al_5Zn_x$ intermetallic top dross and zinc oxide has been developed by POSCO [27]. The POSCO snout process technology utilizes a contact free inducer to apply a drag and levitation force to a snout contaminant to guide contamination away from the production material and towards a collection chamber. The use of an alternating current applied to electromagnets or a rotating permanent magnet to interact with snout surface oxides as a diamagnetic substance would minimise any contamination entrainment within the coating during production and eliminate the arrowhead defect. Furthermore, optimisation of this system to include homogeneous

ACCEPTED MANUSCRIPT

formation of barrier surface oxides on the exposed surface in a wet HNx snout atmosphere would minimise any defects resulting from formation of zinc vapour.

Methods of reducing the impact on surface quality of Zn vapour in a dry HNx snout environment, thus eliminating the requirement for wet HNx injection have been developed [28]. The continuous galvanizing line snout equipped with protective gas exchange system, whereby a series of extraction openings are located adjacent to injection openings on both faces to replace contaminated snout atmosphere with fresh uncontaminated HNx gas. The apparatus is designed with a characteristic injection angle to control the impact between injected gas and the metal substrate and minimise entrainment of the injection gas towards the motel zinc surface. The introduction of this process would obviate the need for wet HNx injection and eliminate the fundamental cause of surface oxide based coating defects.

ACCEPTED MANUSCRIPT

5. CONCLUSION

Whilst the use of wet HNx reduces the formation of zinc dust related defects during continuous galvanizing, the formation of surface barrier oxides can induce other quality concerns. The entrainment of the surface barrier oxide into the zinc coating has resulted in the formation of the arrowhead defect. SEM/EDX characterisation coupled with incremental etching using Nital revealed the presence of the surface contamination within the zinc coating relative to the microfolding which is characteristic of the arrowhead defect. If optimum settings for wet HNx injection/oxide removal are not continually in operation, increased occurrences of coating defects will be observed and result in poor quality full finish material. The presence of the arrowhead defect was shown to reduce the coatings' corrosion resistance by a factor of 2.5. This was illustrated through the use of the Scanning Vibrating Electrode Technique (SVET) which was able to compare zinc mass loss on samples with and without defects. The increase in corrosion rate is due to localised reduction in coating thickness exposing areas of iron which act as sites for cathodic oxygen reduction. This demonstrates that coating defects such as these are more than just aesthetic and lead reductions in coating corrosion resistance. The injection of wet HNx as a method of eliminating the formation of zinc vapour is therefore a "double edged sword" and with the recent development of

ACCEPTED MANUSCRIPT

innovative alternatives to wet HNx injection, coating defects which originate from the formation of zinc vapour and surface barrier oxide can be virtually eliminated.

ACCEPTED MANUSCRIPT

6. ACKNOWLEDGEMENTS

We thank Tata Steel Strip Products and the EPSRC for funding this research under the MATTER Engineering Doctorate Scheme.

ACCEPTED MANUSCRIPT

7. REFERENCES

[1] A.R. Marder, “The metallurgy of zinc-coated steel”, Prog. Mater. Sci., 45 (2000), 198

[2] F. Dunbar, “Defects of the 80’s – A closer look at the critical requirements for today’s hot dip galvanized” Proc. of Galvanizer's association (1988),

[3] Y. W. Kim, S. C. Kung, W. C. Sievert, R. Patil, “Surface defects in exposed quality hot-dip galvanized steel”, Conf. Proc. Galvatech 1989, 120-129

[4] N. Y. Tang and F. E. Goodwin, “A study of defects in galvanized coatings”, Conf. Proc. Galvatech (2001), 49-55

[5] F. Chen, R Patil, "An In depth Analysis of Various Subtle Coating Defects of the 2000's", Conf. Proc. Galvatech, (2004)

[6] A. Azimi, F. Ashrafizadeh, M. R. Toroghinejad, F. Shahriari, “Metallurgical assessment of critical defects in continuous hot dip galvanized steel sheets”, Surf. and Coat. Technol., 206 (21), (2012), 4376-4383

[7] J. L. Arnold, S. L. Boston, F. Caudill, "Control of defects caused by zinc vaporisation in the snout", Conf. Proc. Galvatech, (1989), 130

[8] H. Yamaguchi, T. Hisamatsu, “Reaction Mechanism of the Sheet Galavanizing” Journ. Of the Iron and Steel. Inst. of Japan, 60, 1974, 96.

[9] H. Y. Kim, J.S. Kim, S.J. Lee, "On Decreasing Zinc Dust in Snout equipped CGL", Proc. of Galvanizer's association (2012)

[10] H. Saint-Raymond, S. Gauthier, A. Lamande, “Modelling of zinc vaporisation in snout” Proc. of Galvanizer's association, (2012)

[11] G. C. Becherer, "Utilizing pumps to continuously remove dross from inside the inlet snout", Proc. of Galvanizer's association, (2001)

[12] C. Phillips, N. Staples, M. Bright, "Cleanliness Enhancement of the Bath Surface within a CGL snout", Proc. of Galvanizer's association, (2005)

[13] D. Dauchelle, H. Baudin, L. Gacher, Y. Prigent: Method & installation for dip coating of a metal strip, U. S. Patent No. 6,936307 (Aug. 30, 2005)

[14] G. Vourlias, N. Pistofidis, G. Stergioudis, E. Polychroniadis, "An overview of the solid byproducts of the galvanizing kettle", Optoelectron. and Adv. Mat., 1, (2007), 77-85

[15] G. Vourlias, K. Pistofidis, G. Stergioudis. E. Polychroniadis, "A negative effect of insoluble particles of dross on the quality of the galvanized coatings" Solid State Sci., 7 (2005), 465 – 474

[16] D. Penney, J. Sullivan, D. Worsley, "Investigation into the effects of metallic coating thickness on the corrosion properties of ZnAl alloy galvanizing coatings" Corr. Sci, 49, 3, (2007), 1321 – 1339

[17] H. McMurray, D. Worsley, "Scanning techniques for Monitoring Localised Corrosion Phenomena", Rev. Chem. Kin. 4, (1997), 149

[18] J. Sullivan, C. Weirman, J. Kennedy, D. Penney, "Influence of Steel Gauge on the Microstructure and Corrosion Performance of Zinc Alloy Coated Steels", Corr. Sci, 52 (2010) 1853-1862

[19] M. Vlot, C. Price, M. Zuijderwijk, B. Van Veldhuizen, "Full Finish GI Manufacturing for the automotive industry", Conf. Proc. Galvatech, (2004)

[20] M. Zelechower, J. Klis, E. Augustyn, J. Grzonka, D. Stroz, T. Rzychon H. Woznica, "The mircostructure of annealed galfan coating on steel substrate", Arch. of Metall. and Mater., 57, (2012), 517-523

[21] S. Alam, M. Poloju, S. Sahu, M. Kumar, A. Singh, "SEM, EDX & XRD of Zinc Oxide Nanostructures synthesized by Zinc oxidation", Microsc. and Anal., 06, (2012), 11-14

[22] E. M. A. Jamal, D. S. Kumar, M. R. Anatharaman, "On structural, optical and dielectric properties of zinc aluminate nanoparticles" Bull. of Mater. Sci., 34, (2007), 251-259

[23] G. Ragul, S. Sumathi, "Synthesis, Characterisation and Photocatalytic study of Zinc Aluminate Nanopowders against Rhodamine -B and Crystal Violet Dyes" Int. J. of Appl. Eng. Res., 8, (2013), 2175-2178

[24] C. Cheng, H. J. Fan, "Branched nanowires: Synthesis and energy applications", Nano Today, 7, (2012). 327-343

[25] S. Xu, Z. L. Wang, "One-Dimensional ZnO Nanostructures: Solution Growth and functional properties" Nano Res., 4, (2011), 1013-1098

[26] S Y. Pung, W P. Lei, A. Aziz, "Kinetics of organic dye degradation usuing ZnO particles with different morphologies as a photocatalyst", Int. Journ. Inorg. Chem., 2012 (2012), 1-9

ACCEPTED MANUSCRIPT

[27] T. I. Jang, Y. H. Kweon, J. K. Kim, C. W. Jee, "Apparatus for removing pollutant source from snout of galvanizing line", U. S. Patent No. 9133540 (September 15, 2015)

[28] N. Schaffrath, S. Zeizinger, M. Peters, G. Nothacker, K. Peters: "Method and device for avoiding surface defects caused by zinc dust in a continuous strip galvanising process patent", U. S. Patent No. 0167138 (Jun 18, 2015)

ACCEPTED MANUSCRIPT

8. FIGURE CAPTIONS

Table 1 – Elemental bath composition during GI Full Finish production and associated production parameters

Figure 1 – Schematic of the Continuous galvanizing line snout indicating the relationship between a dry & wet HNx atmosphere & the formation of Zn vapour

Figure 2 – Time-lapse image from snout camera highlighting the entrainment of surface oxides into the zinc coating. Central light and dark regions are uncontaminated molten zinc with surface contamination present at the extremities of the snout, which are seen to be moving towards the steel substrate resulting in entrainment of contamination into the coating

Figure 3 – Arrowhead defect image taken from Galvanizing line quality inspection system

Figure 4 – Backscatter image highlighting compositional variation within coating relative to characteristic zinc microfolding

Figure 5 - Schematic illustrating the formation of the arrowhead defect indicating the entrainment of snout surface oxide and its break up when subject to high velocity wiping

Figure 6 – White light interferometry 3d surface map indicating surface topography with associated Ra for arrowhead defective and non-defective material

Figure 7 – SEM image of GI Full Finish steel cross section highlighting a contamination free Fe_2Al_5 interfacial layer

Figure 8 – SEM image of GI Full Finish steel cross section/EDX spectra highlighting the presence of oxide based contamination relative to Zn coating/substrate interface

Figure 9 – SEM image of etched GI Full Finish surface/EDX mix colour map highlighting presence of oxide contamination within coating relative to microfold Where Green = Al, Red = O, Blue = Zn

Figure 10 – SEM image of etched GI Full Finish surface/EDX surface colour mapping of individual chemical constituents highlighting presence of intermetallic $Fe_2Al_5Zn_x$ top dross particle entrained with tail of the defect

Figure 11 – XRD diffractogram comparing head end and tail end chemical composition of the arrowhead defect

Figure 12 – Cumulative Zn mass loss of arrowhead v non defective GI Full Finish material

Figure 13 – SVET Current density mapping of arrowhead defective material, where red = anodic activity (zinc oxidation), blue = cathodic activity (oxygen reduction)

Figure 14 – SEM image of complex morphologies comprising white snout surface oxide produced on a molten zinc surface through the injection of wet HNx

Figure 15 – SEM image of microstructural phenomena of snout contamination/EDX mix colour map highlighting presence of Zn & O. Where Green = Al, Red = O, Blue = Zn

Figure 16 – SEM image of ZnO based coarse and fine nanorods formed though injection of wet HNx

Figure 17 – XRD diffractogram of white ZnO surface oxide snout contamination

Figure 18 – XRD diffractogram of Arrowhead defective and non-defective GI Full Finish at a 25 Primary optic incidence angle

Figure 19 – Monthly % rejection chart for arrowhead defective material pre and post modification of snout cleanliness control practice

ACCEPTED MANUSCRIPT

ACCEPTED MANUSCRIPT

9. FIGURES

Table 1

Element	Bath Composition (wt%)	Bath temperature (°C)	Line speed (m/min)	Strip entry temperature (°C)
Zn	99.7	465	1.5	475
Al	0.3			
Al_{eff}	0.3			
Fe	0.008			

Figure 1

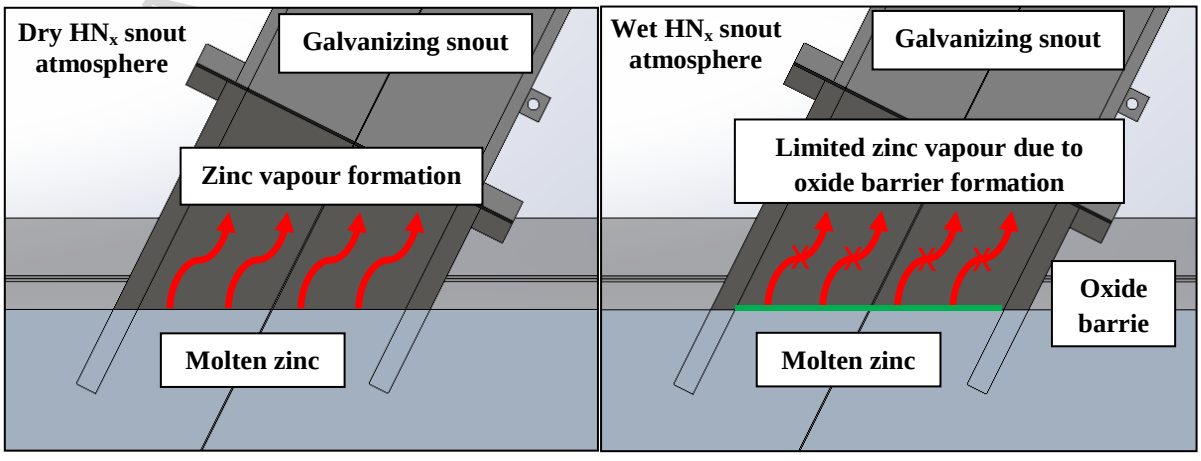

Figure 2

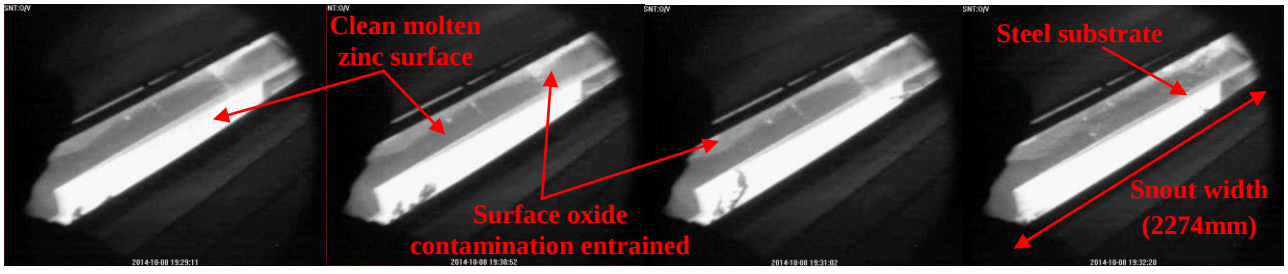

Figure 3

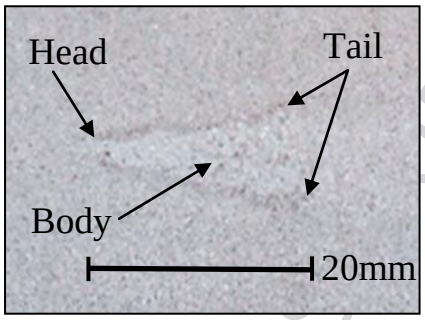

Figure 4

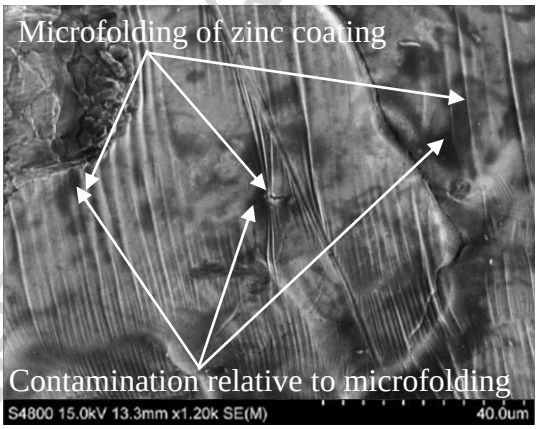

Figure 5

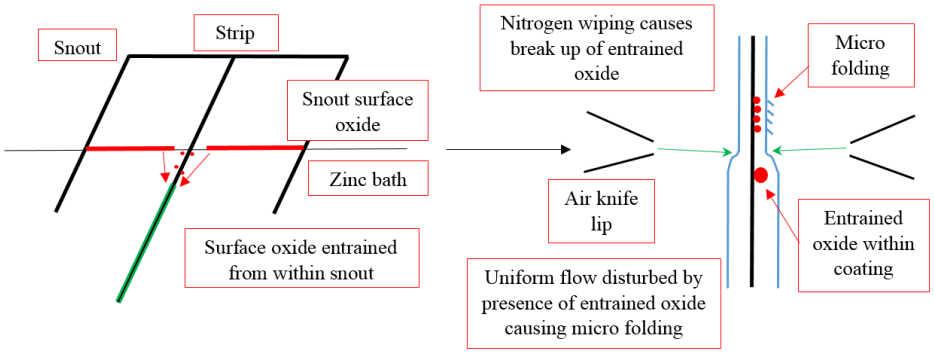

Figure 6

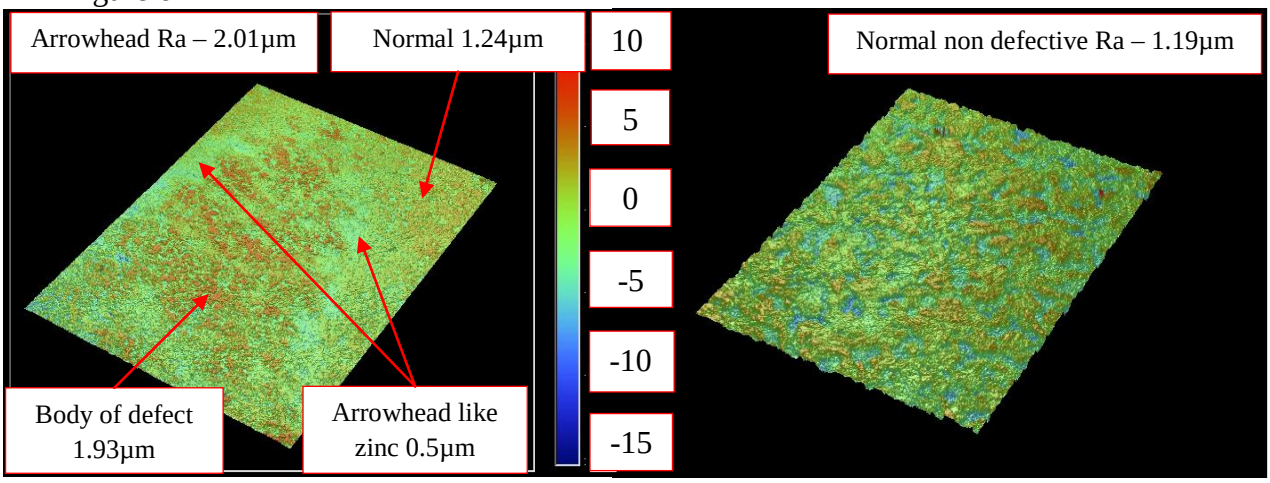

Figure 7

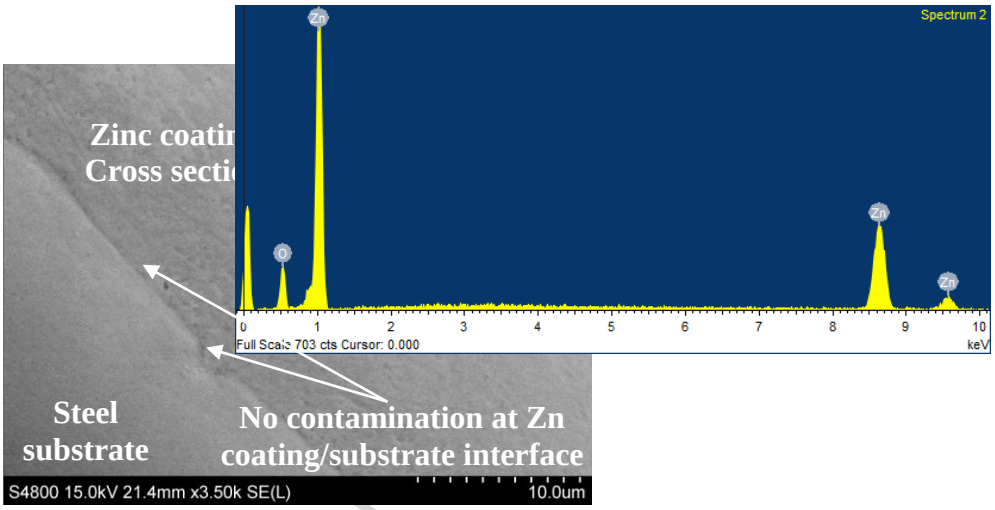

Figure 8

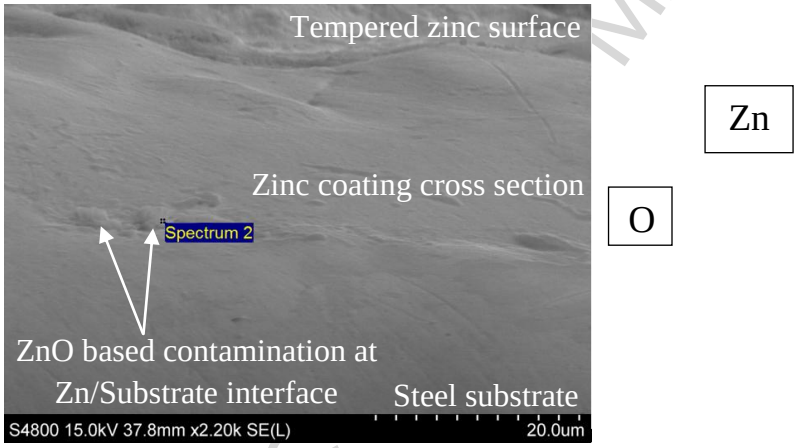

Zn

O

Figure 9

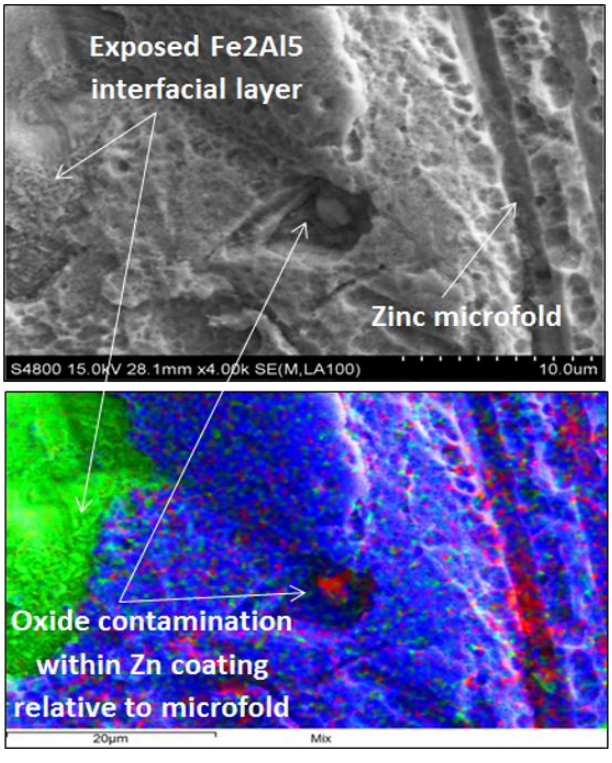

Figure 10

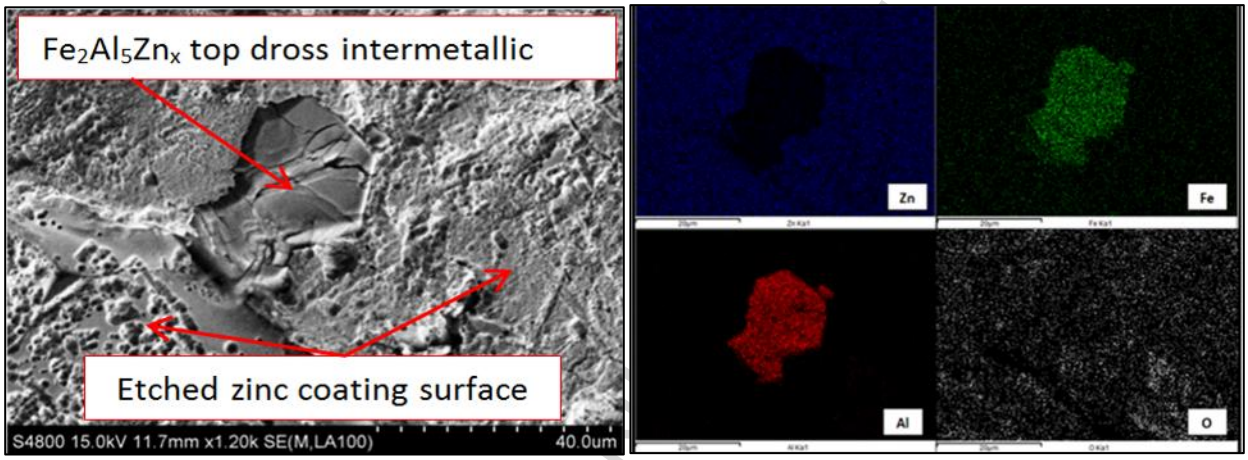

Figure 11

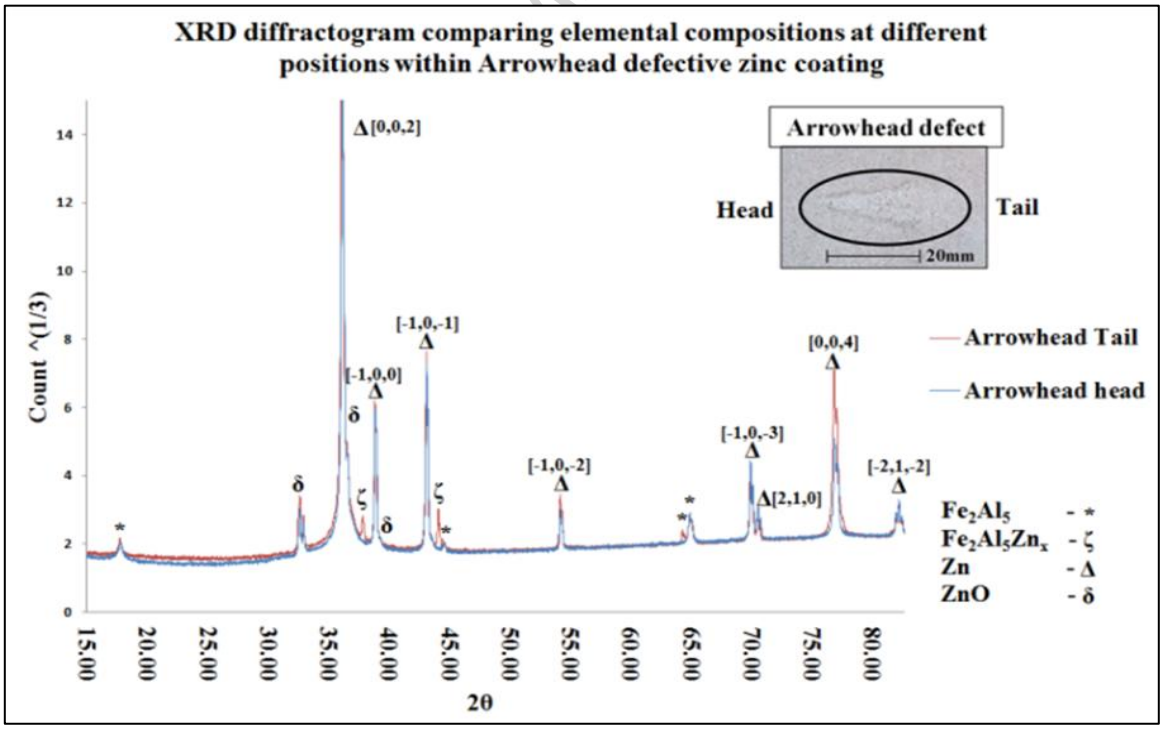

Figure 12

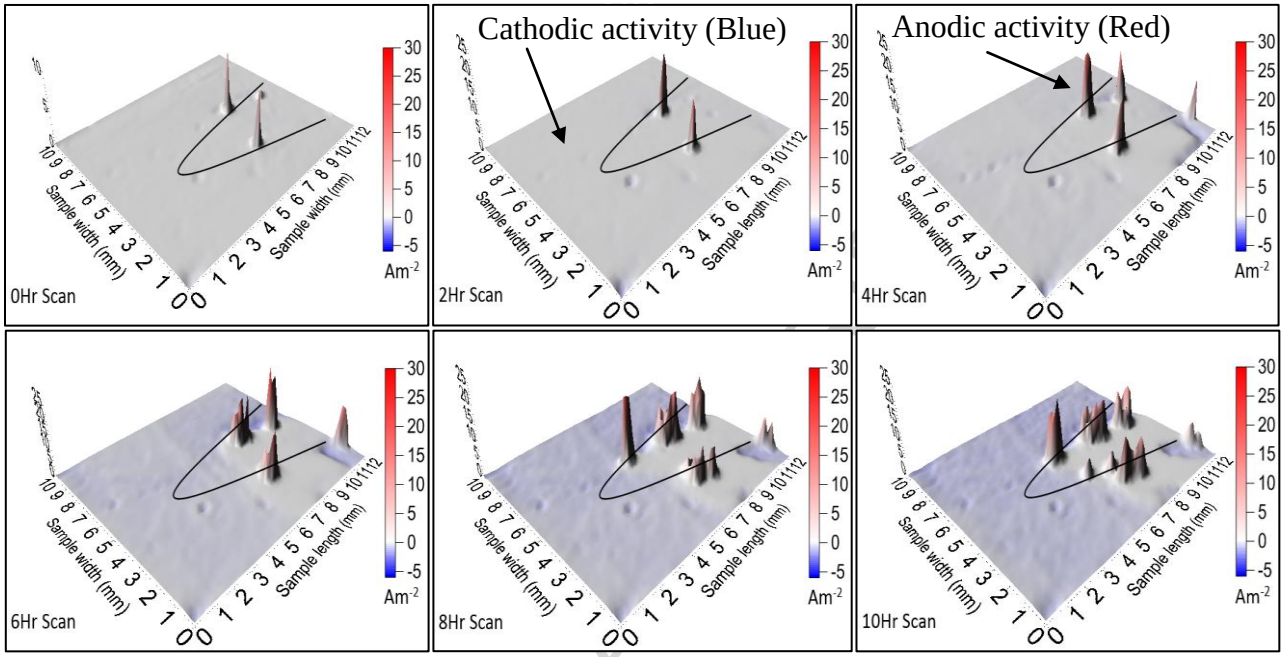

ACCEPTED MA

Figure 13

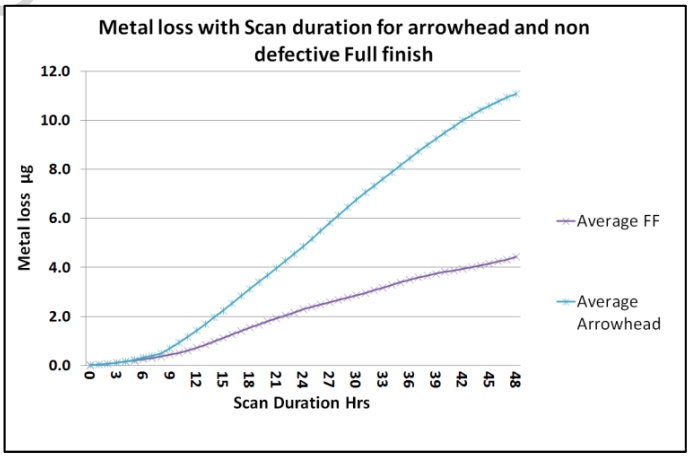

Figure 14

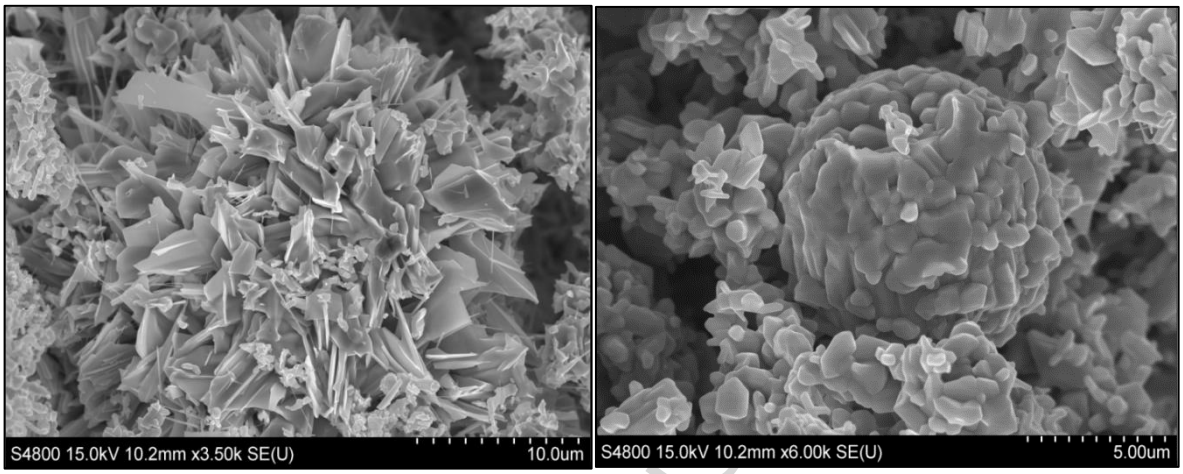

Figure 15

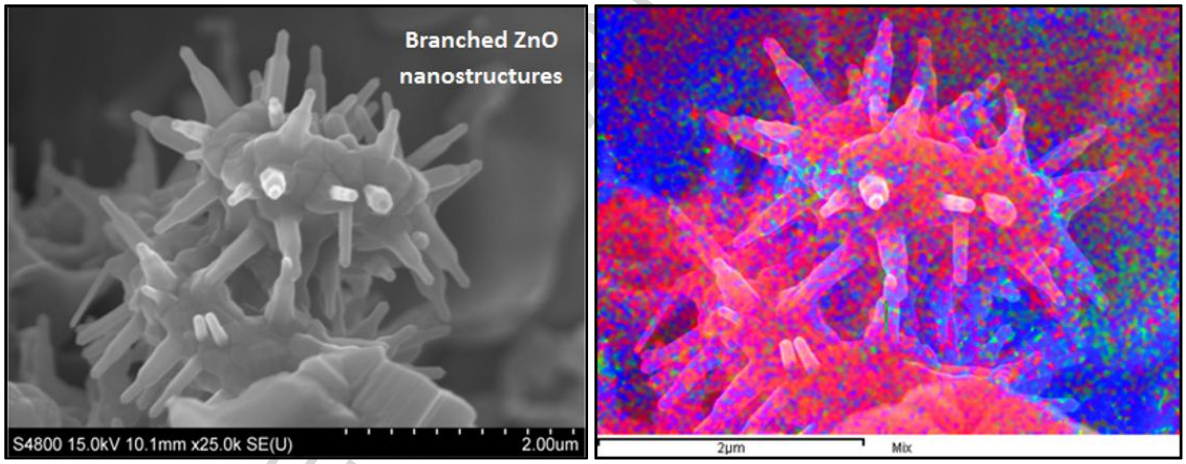

ACCE

Figure 16

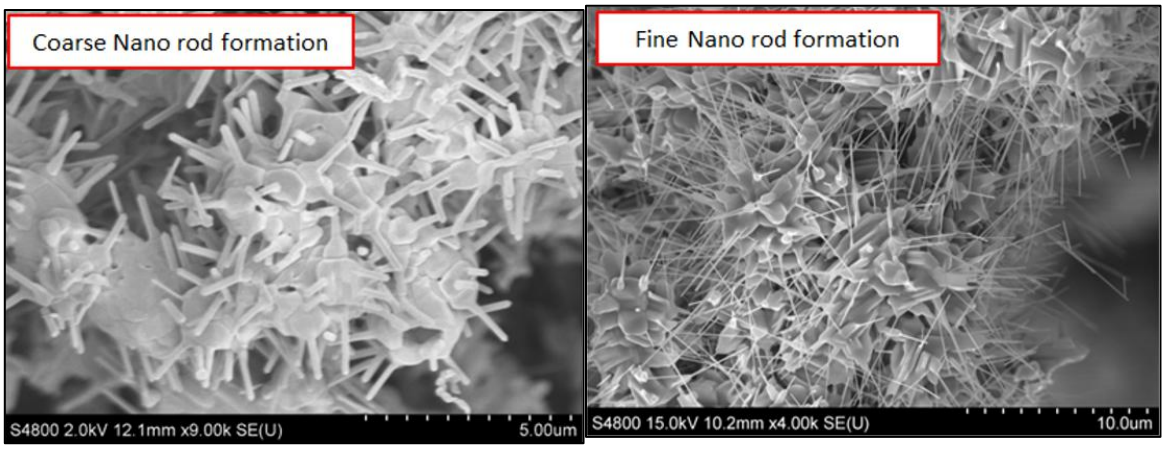

Figure 17

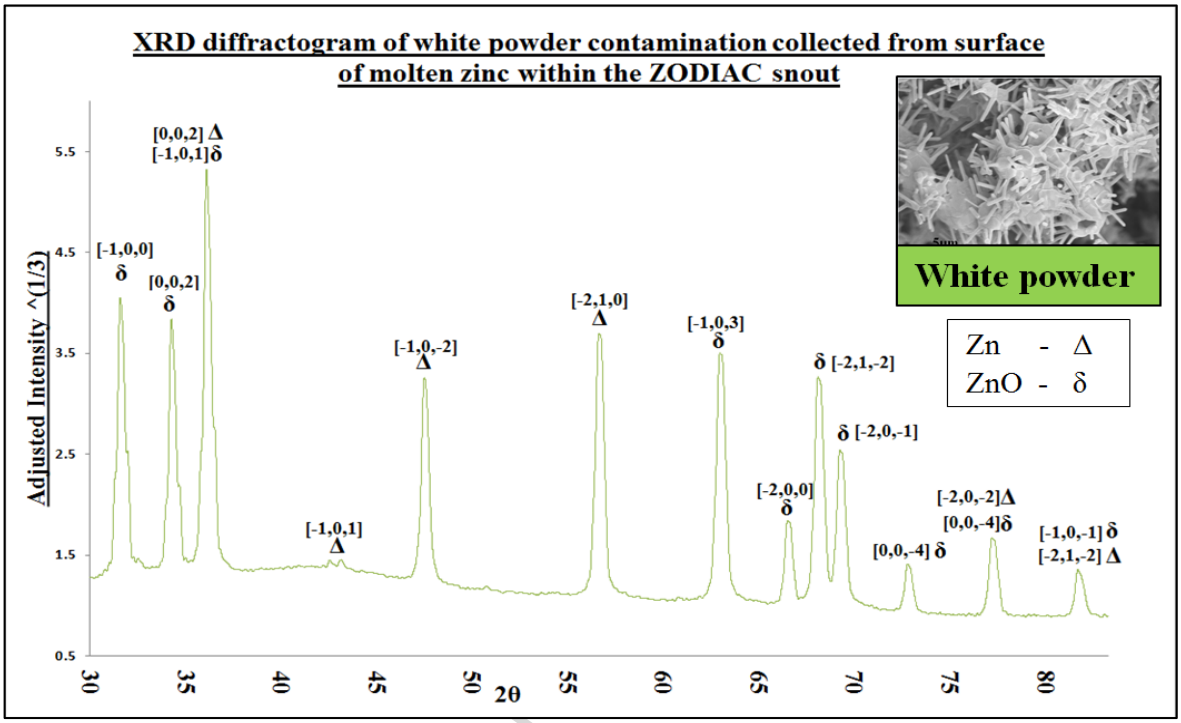

ACCEPTED

Figure 18

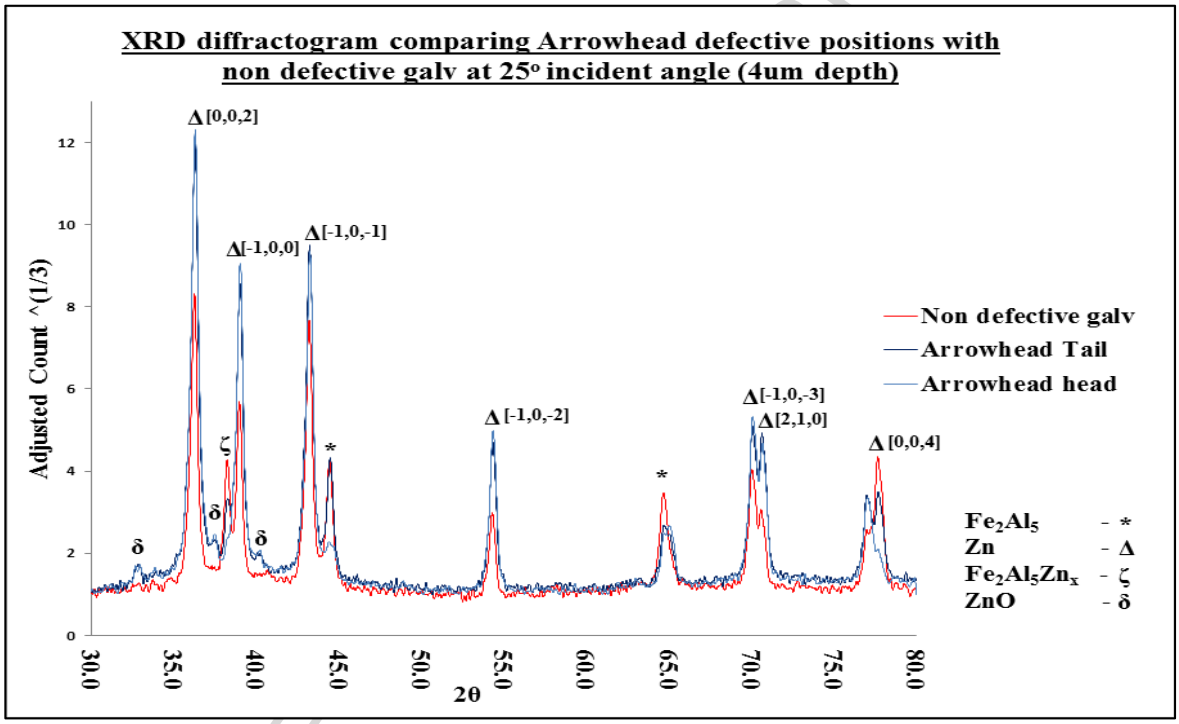

ACCEPTED MANUSCRIPT

Highlights

- Metallographic and chemical characterisation of novel arrowhead oxide defect
- Fixed incidence diffractograms highlight the presence of ZnO within defective regions of the coating
- Mechanism of formation deduced based on chemical characteristics and surface topography of defect
- Novel nanowire ZnO formation as by-product of continuous hot dip galvanizing
- Methods of eliminating the use of wet HNx injection as a method for suppressing Zn vapour formation presented

ACCEPTED MANUSCRIPT